Supporting Information

Recyclable Nanographene-based Micromachines for the On-the-Fly Capture of Nitroaromatic Explosives

*Bahareh Khezri, Seyyed Mohsen Beladi Mousavi, Zdeněk Sofer, Martin Pumera**

E-mail: martin.pumera@vscht.cz

Video S1. presents the motion of the n-rGO/Ni/Pt without magnet

Video S2**.** presents the motion of the n-rGO/Ni/Pt with magnet control

(a)

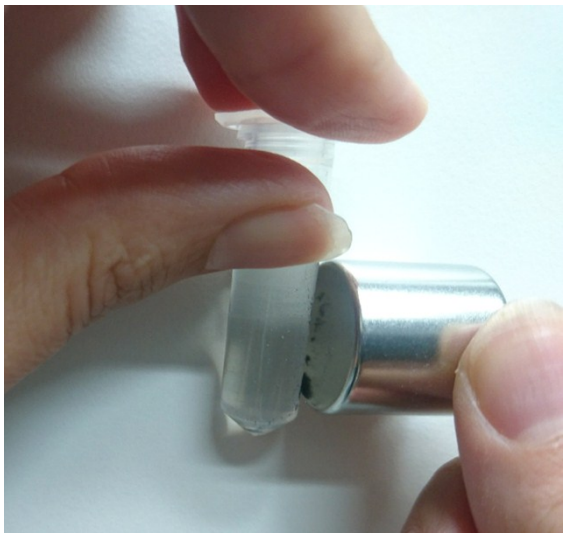

(b)

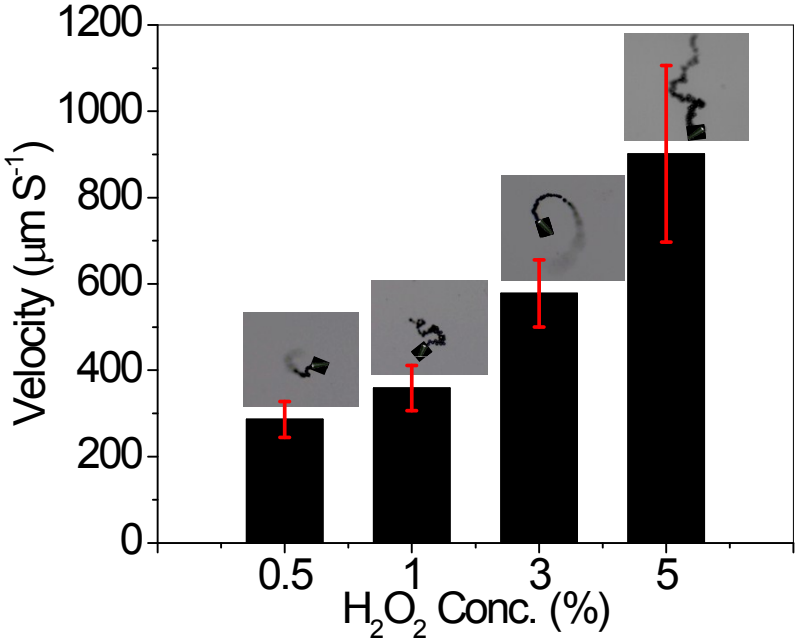

Figure S1. The impact of fuel concentration on average velocity. Presented speed is the average of 20 independent tests. Error bars show the standard deviation for speed measured at each concentration of fuel (H_2O_2). All motion analyses were carried out at a constant sodium dodecyl sulfate (SDS) concentration (0.5 %).

Figure S1. presents the Propulsion of n-rGOx/Ni/Pt micromachines in the presence of different concentration of the fuel 0.5%, 1%, 3% and 5% H_2O_2.

Removal of NACs

To study the remediation capability of n-rGO/Ni/Pt micromachines, they were used for removal of NACs from contaminated solutions. Micromachines (10^6 motors mL^{-1}) propelled (in the presence of 1% H_2O_2 and 0.5% SDS) in 1 ml of contaminated solutions (TNP (25 mg/l) or DNT (100 mg/l)) for 1, 2, 3, 5, 10 and 15 minutes to catch the target explosive compounds. As it can be seen in **Figure S2**, UV-Vis analysis of contaminants (TNP and DNT) have demonstrated a dramatic decrease corresponding to 92.1 ± 3.7 and 90.1 ± 2.9% removal of TNP and DNT respectively.

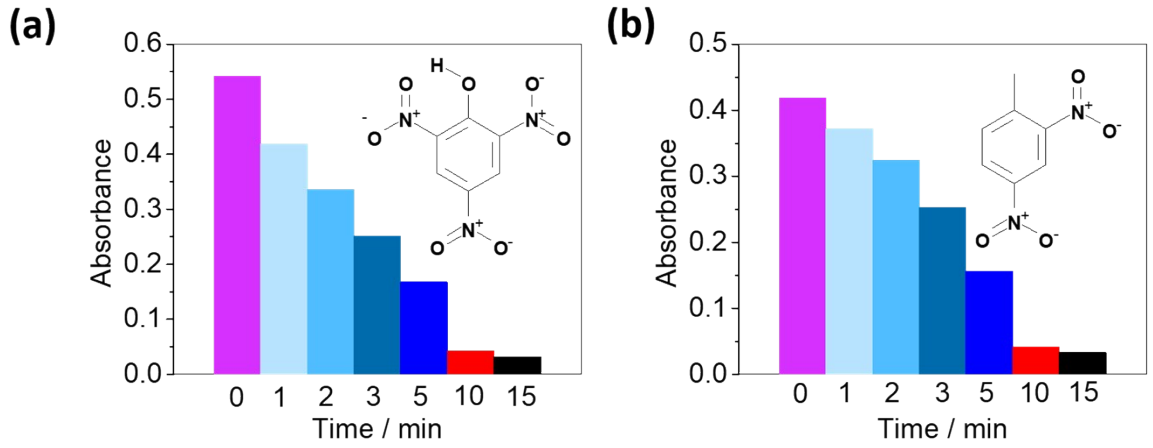

Figure S2. Time dependence of the removal of different NACs: (a) TNP (wavelength : 357 nm) and (b) DNT (wavelength : 240 nm)

To study the crucial role of micromachine movement, control experiments were performed using static (absence of H_2O_2) and magnet-guided micromachines to capture NACs, then the results compared with bubbled-propelled micromachines. Their corresponding UV-Vis spectrums and electrochemical responses have been demonstrated in **Figure S3.a-b** (TNP) and **Figure 4S.a-b** (DNT). Section **c** in **Figures S3** and **S4** presents the removal efficiency of the dynamic micromachines compared with static and magnet-guided micromachines after 10 minutes contact with contaminants. In the absence of hydrogen peroxide, micromachines immersed in contaminated water showed a negligible removal (< 10%) while removal efficiency increased to 23-37% for magnet-guided micromachines. The comparison of removal efficiency for magnet-guided and bubble-propelled micromachines reveals that higher speed of bubble-propelled micromachines leading to a higher decontamination efficiency that could be the result of the enhanced diffusion and the higher chance of interaction.

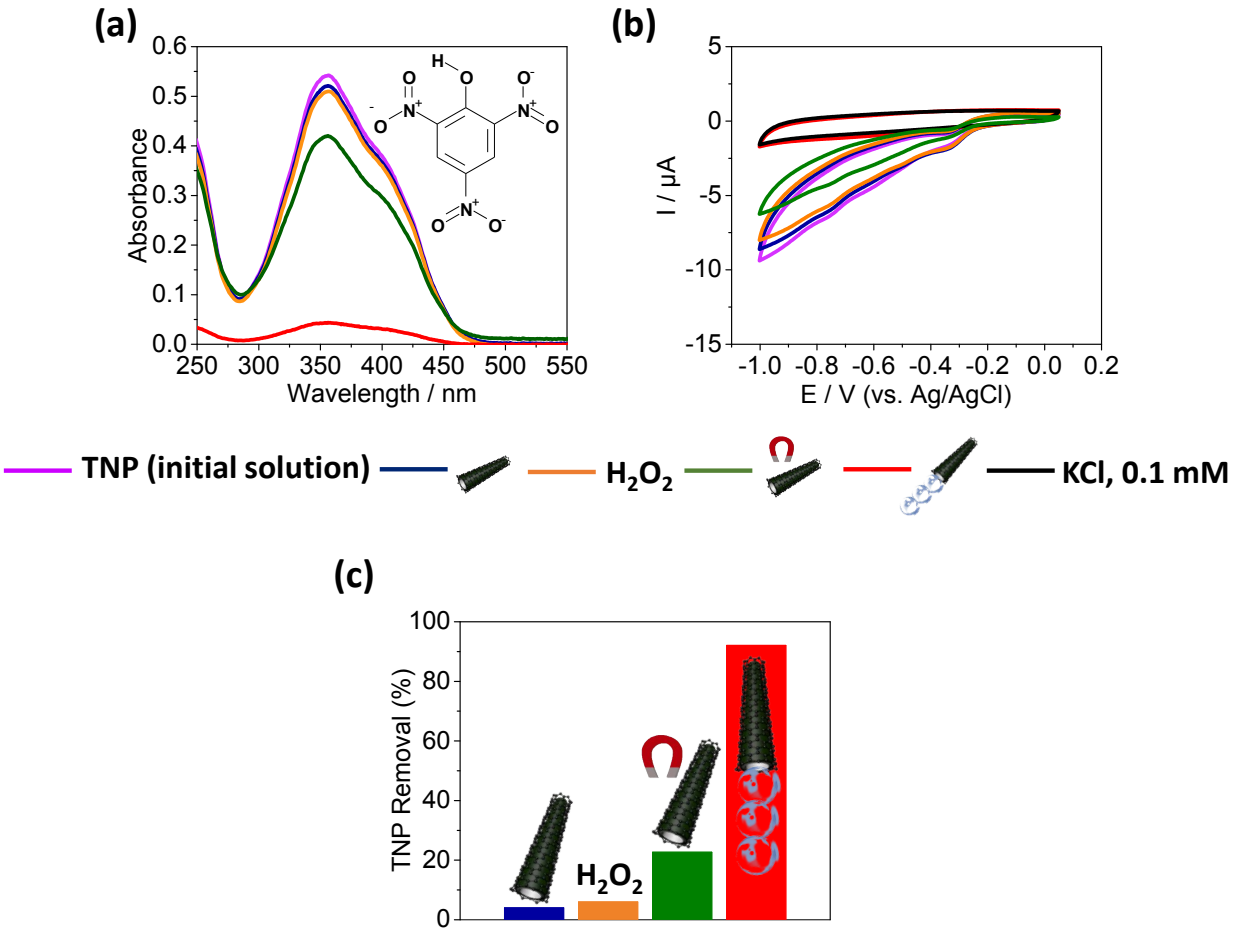

Figure S3. Removal of TNP on the n-rGO/Ni/Pt micromachines: TNP adsorb physically on the outer layer of micromachine (n-rGO). (a) The UV-Vis spectra of TNP solution prior and after 10 minutes adsorption on the n-rGO/Ni/Pt micromachines. (b) Electrochemical response of TNP solution prior and after 10 minutes adsorption on the n-rGO/Ni/Pt micromachines (conditions: Scan rate: 50 mV s^{-1}, Electrolyte: 0.1 mM KCl, reference electrode (RE): Ag/AgCl and counter electrode (CE): Pt wire). For both optical and electrochemical responses, control experiments including static micromachines, magnetic-guided micromachines and the impact of fuel (H_2O_2) have been compared in same graphs. (c) Removal of TNP in different system: bubble-propelled n-rGO/Ni/Pt micromachines (fuel: H_2O_2, 0.5%) showed removal efficiency of 92.1% while for magnet-guided micromachines (absence of fuel, using an external magnet), it decreases to 22.7%. Performing the experiment using static n-rGO/Ni/Pt micromachines (absence of fuel and external magnet) resulted removal efficiency of 4.0%. The study of the impact of fuel (absence of micromachines) showed the removal efficiency of 6.0% in concentration level of 1% H_2O_2.

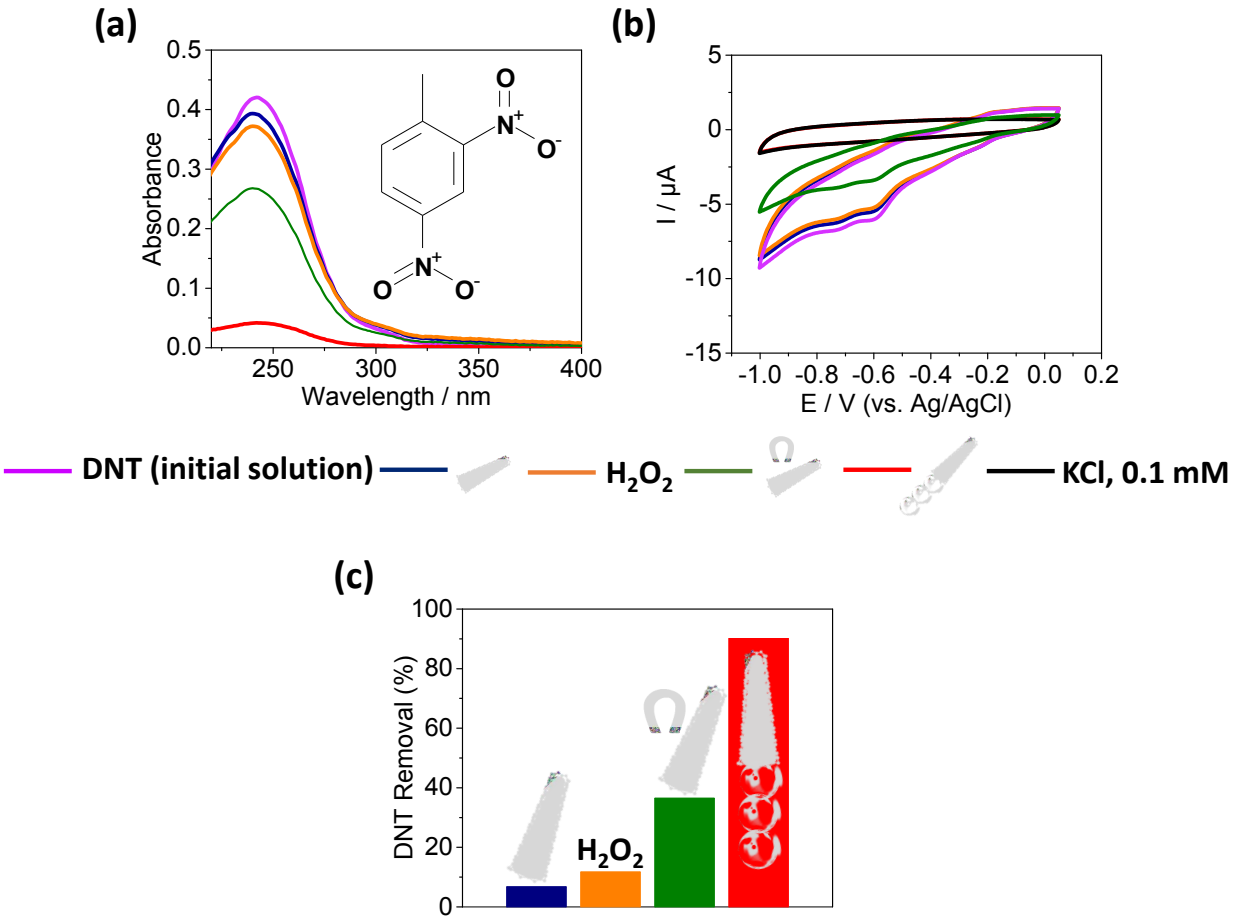

Figure S4. Removal of DNT on the n-rGO/Ni/Pt micromachines: DNT adsorb physically on the outer layer of micromachine (n-rGO). (a) The UV-Vis spectra of DNT solution prior and after 10 minutes adsorption on the n-rGO/Ni/Pt micromachines. (b) Electrochemical response of DNT solution prior and after 10 minutes adsorption on the n-rGO/Ni/Pt micromachines (conditions: Scan rate: 50 mV s^{-1}, Electrolyte: 0.1 mM KCl, reference electrode (RE): Ag/AgCl and counter electrode (CE): Pt wire). For both optical and electrochemical responses, control experiments including static micromachines, magnetic-guided micromachines and the impact of fuel (H_2O_2) have been compared in same graphs. (c) Removal of TNP in different system: Bubble-propelled n-rGO/Ni/Pt micromachines (fuel: H_2O_2, 0.5%) showed removal efficiency of 90.1% while for magnet-guided micromachines (absence of fuel, using an external magnet), it decreases to 36.5%. Performing the experiment using static n-rGO/Ni/Pt micromachines (absence of fuel and external magnet) resulted removal efficiency of 6.7%. The study of the impact of fuel (absence of micromachines) showed the removal efficiency of 11.0% in concentration level of 1% H_2O_2.

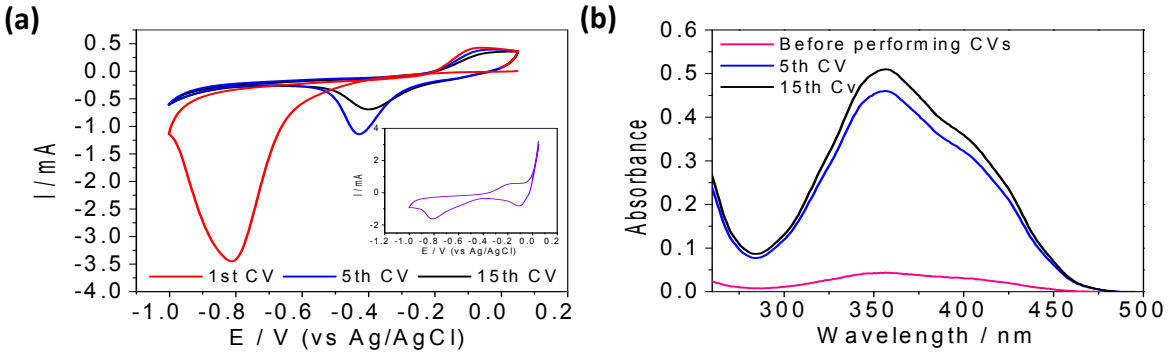

Figure S5. Electrochemical regeneration of n-rGO/Ni/Pt micromachines; (a) electrochemical triggered TNP release from n-rGO/Ni/Pt micromachines, inset: TNP CV in KCl (condition: scan: 0.0 ↔ −1.0 V, electrolyte: 0.1 mM KCl, scan rate: 50 mV in all CVs). (b) UV-Vis spectra of the solution before performing the release procedure (pink) and after (blue: 5th CV and black: 15th CV) confirming successful electrochemical triggered release.

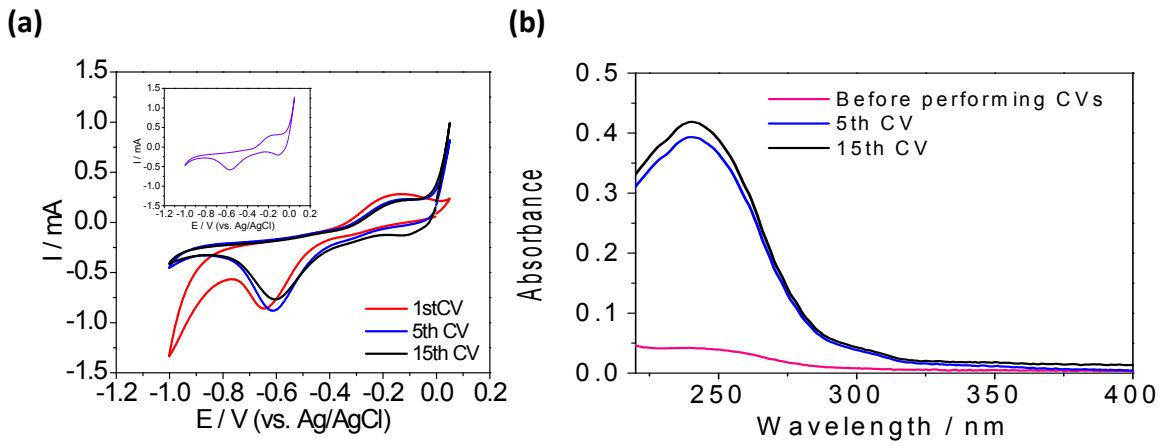

Figure S6. Electrochemical regeneration of n-rGOx/Ni/Pt micromachines; (a) electrochemical triggered DNT release from n-rGOx/Ni/Pt micromachines, inset: DNT CV in KCl (condition: scan: 0.0 ↔ −1.0 V, electrolyte: 0.1 mM KCl, scan rate: 50 mV in all CVs). (b) UV-Vis spectra of the solution before performing the release procedure (pink) and after (blue: 5th CV and black: 15th CV) confirming successful electrochemical triggered release.

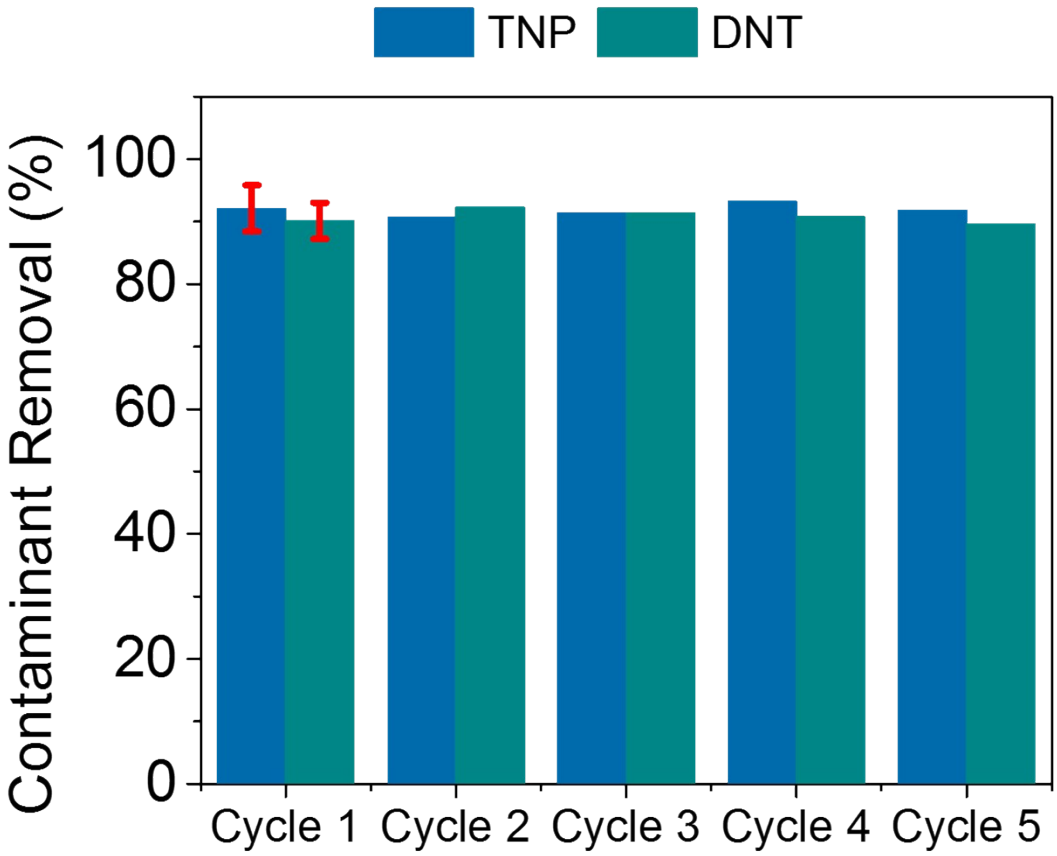

Figure S7. Reusability of n-rGOx/Ni/Pt micromachines, representing TNP and DNT removal in five cycles with same batch of micromachines. In all five cycles, contaminant loaded-micromachines collected and regenerated electrochemically. After washing, they used for the next contaminant removal experiment. Experimental conditions for contaminant removal: 1.0% (v/v) of H_2O_2 and 0.5% (w/v) of SDS. Error bars in first cycle calculated using repentance of contaminant removal experiment with three different batch of n-rGOx/Ni/Pt micromachines.

Table S1. Carbon-based micromachines for removal of pollutants.

Machine	Composition	Pollutant	Condition	Recycling	Ref
	activated carbon/Pt	2,4-dinitrotoluene/Lead/methyl paraoxon/Rhodamine 6G	RT[a]: 5 FC[b]: 2 U[c]: 190 ± 60 RE[d]:96/90/92/92 NO.[e]: 1.0×10^{6}	-	[1]
	GOx/Ni/Pt	Lead	RT: 60 FC:1.5 U: 500 RE:83-95 NO.: 2.0×10^{5}	Using HNO_3	[2]
	ZrO_2-erGO/Pt	methyl paroxon/ethyl paraoxon/bis-4 nitrophenyl phosphate	RT: 5 FC: 1.5 U: 450 ± 80 RE: 91 NO.: 1.0×10^{6}	-	[3]
	SiO_2@rGO/Pt	Polybrominated diphenyl ethers/5-chloro-2-(2,4-dichlorophenoxy) phenol	RT: 10 FC: 1.5% U: 140±15 RE:91/87 NO.: 1.5×10^{6}	Using an isooctane solvent	[4]
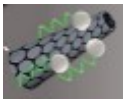	FAM-Ricin B aptamer-rGO/Pt	Ricin B toxin	RT: 3 FC: 1 U: 380 RE: 65-90	-	[5]
	rGO/PtNPs	Fumonisin B1/ocratoxin A	RT: 2 FC: 1 U: 360±60 RE: 96-98	-	[6, 7]
	Pt/GO	tetracycline	RT: 30 FC: 1 U: RE: 96 NO. 2.0×10^{3}		[8]
	n-rGO/Ni/Pt	2,4,6-trinitrotoluene/2,4,6-trinitrophenol/2,4-dinitrotoluene	RT: 10 FC: 1 U: 350 RE: 90-92 NO. 1.0×10^{6}	Electrochemical regeneration	this work

RT: recovery time (minutes), b) FC: fuel concentration (% v/v), c) U: velocity: (μm s^{-1}), d) RE: removal efficiency (%), e) NO.: number of motors per ml

1. Jurado-Sánchez, B., et al., *Self-Propelled Activated Carbon Janus Micromotors for Efficient Water Purification.* Small, 2015. **11**(4): p. 499-506.
2. Vilela, D., et al., *Graphene-Based Microbots for Toxic Heavy Metal Removal and Recovery from Water.* Nano Lett., 2016. **16**(4): p. 2860-2866.
3. Singh, V.V., et al., *Zirconia/Graphene Oxide Hybrid Micromotors for Selective Capture of Nerve Agents.* Chem. Mater., 2015. **27**: p. 8162-8169.
4. Orozco, J., et al., *Graphene-based Janus micromotors for the dynamic removal of pollutants.* J. Mater. Chem. A, 2016. **4**: p. 3371-3378.
5. Esteban-Fernández de Ávila, B., et al., *Aptamer-Modified Graphene-Based Catalytic Micromotors: Off–On Fluorescent Detection of Ricin.* ACS Sens., 2016. **1**: p. 217-221.
6. Molinero-Fernández, Á., et al., *Biosensing Strategy for Simultaneous and Accurate Quantitative Analysis of Mycotoxins in Food Samples Using Unmodified Graphene Micromotors.* Analytical Chemistry, 2017. **89**(20): p. 10850-10857.
7. Molinero-Fernández, Á., et al., *Magnetic Reduced Graphene Oxide/Nickel/Platinum Nanoparticles Micromotors for Mycotoxin Analysis.* Chem. Eur. J., 2018. **24**: p. 7172-7176.
8. Dong, Y., et al., *A substrate-free graphene oxide-based micromotor for rapid adsorption of antibiotics.* Nanoscale, 2019. **11**(10): p. 4562-4570.